Ghost Imaging: Venturing into New Experimental Frontiers

S-Proj Mid Report

Hania Shahid

24100044

Abstract

Recent advances in quantum imaging experimentation have led to the idea and realization of quantum holography. What we try to remodel in the photon laboratory is a cost-effective and re-envisioned way to conduct experiments regarding quantum ghost imaging.

Contents

1 Introduction

One of the most significant phenomena that has been realized in the laboratory regarding quantum mechanics is quantum imaging. Quantum imaging is one of the consequences of quantum entanglement. Furthermore, it has recently become a 'hot topic' in the photonics community.

Quantum imaging leverages quantum properties such as entanglement, superposition, and quantum state measurement to obtain imaging data that would be difficult or impossible to achieve with classical imaging methods. It allows us to reproduce classical imagine effects in a non-local fashion, using entangled photon pairs and coincidence counting entangled photons produced using spontaneous parametric down-conversion. One of the forms of quantum imaging has been named ghost imaging. In this method, two entangled light beams are used. One beam illuminates the object and does not reach the detector directly, while the second, entangled beam never interacts with the object but is measured by a detector. The image is formed by correlating the measurements from both beams.

Quantum ghost imaging has many advantages over classical methods of imaging. For one, there is an increased signal-to-noise (SNR) ratio. This is because a two-photon entangled beam is far more robust against classical forms of attenuation [1]. Moreover, ghost imaging is effective in low-light conditions, in which classical imaging would be almost impossible. Lastly, if the technique of ghost imaging is applied to larger systems, it offers a much greater level of security as intercepting the quantum states used in imaging can disrupt the information, making eavesdropping detectable[2].

In this exposition, we will be attempting to recreate previous ghost imaging experiments using a simpler and more cost-effective method. The aim is to demonstrate a phenomena of quantum entanglement as well as quantum imaging while also making use of the classical properties of light and obtain the same level of experimental accuracy and further extrapolate the laboratory results. The way we make this experiment more cost-effective than its counterparts [1], [3] is by using bucket avalanche photodiode (APD) detector rather than a single photon detector/camera. A prevalent objective in ghost imaging is to reconstruct images with optimal resolution and minimal acquisition times. However, a notable limitation in ghost imaging lies in its inefficient imaging speed. The speed of imaging is contingent on the number of measurements necessary for image reconstruction, a parameter that scales quadratically with the desired resolution. Additionally, we aim to enhance our results by leveraging AI-based models, thereby increasing the applicability of this experiment. A more in-depth precursor is provided in the following section.

2 Ghost Imaging

Ghost imaging is an unconventional method of capturing images that relies on the correlations between two distinct spatial light fields to generate an object's image. This process involves utilizing photons that have not directly interacted with the object. Each individual light field alone does not provide any image information about the object. However, by examining the correlations between these fields, it

becomes possible to reconstruct an image. Originally demonstrated as a quantum entanglement phenomenon and linked to spontaneous parametric down-conversion (SPDC), ghost imaging has more recently been observed with entanglement swapped photons and symmetry-engineered quantum states [4]. The advantageous use of photons rather than classical light facilitates imaging at low light levels, showcasing an elevated signal-to-noise ratio. The GI reconstruction process often introduces a significant background, leading to the suppression of the signal, resulting in a low-quality reconstructed image. To enhance this, numerous studies employ the calculation of joint probability distributions in the imaging process. This approach aims to improve the signal-to-noise ratio for more accurate and higher-quality reconstructed images.

Motivation

2.1 Preliminaries

We start with some rather fundamental experiments to investigate the more basic quantum properties of light, such as its particle nature and the ability of photon pairs to get entangled and exhibit non-local realism [5].

To check for the quantum nature of light, we employ the setup in figure 1. Down-conversion can be acquired if we superimpose 2 BBO crystals, wherein one of them is aligned at 90^o with respect to the other. This causes an incoming photon in the state $|H\rangle$ to emerge as $|VV\rangle$ (two vertically polarized photons) and vice versa. To carry out fine alignment of the detectors the tilt of the detectors is adjusted using the rotating knobs of the mounts until both the individual until coincidence counts were maximized.

Coincidence counting involves the simultaneous detection of two or more particles at separate detectors. In the realm of quantum mechanics or quantum optics experiments, an economical approach to coincidence counting is implemented using a Field-Programmable Gate Array (FPGA) with an internal clock set at 50 MHz. This configuration allows for an effective coincidence window of 2×10 ns, offering an efficient and cost-effective solution for concurrently counting single and coincident photons across multiple photodetectors. Photons are deemed coincident if they reach different detectors within a specified time coincidence window, in our case, 10 ns. Notably, owing to the independence of the arrival sequence of pulses, the actual coincidence window is precisely twice the width of the pulses. In our specific setup, this window spans 10 ns.

Once we have successfully controlled the polarization of light and completed the down-conversion of photons, the next critical step involves validating the photonic behavior of light. To achieve this, we incorporate a polarizing beam splitter (PBS) into the experimental setup, positioned approximately 3-4 inches from detector B. It is crucial to ensure that the PBS is oriented perpendicularly to the incoming photon beam. The PBS serves the purpose of splitting the beam into two components: a horizontally polarized reflected ray and a vertically polarized transmitted ray. Subsequently, one of these rays is directed into detector B, while the other is routed to detector B'.
To further manipulate the polarization state and gather insightful data, an additional half-wave plate (HWP) is introduced between the BBO crystal and detector B. This configuration allows us to fine-tune the polarization characteristics of the incoming

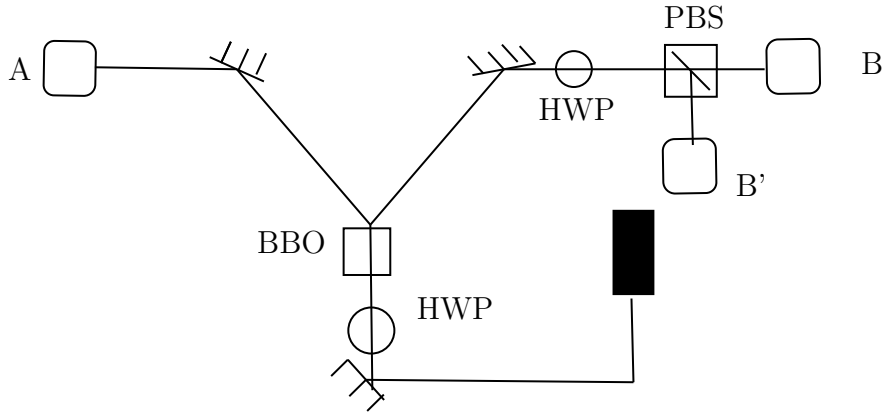

Figure 1: Setup to check for the particle nature of light. The black filled box is our laser. A, B, and B' are bucket detectors. We make use of two half-wave plates. The polarizing beam splitter is used to send half the photons to detector B and the other half to B'.

photons.

Throughout the experimentation process, counts from detectors A, B, and B', as well as coincidence counts such as AB, AB', BB', and ABB', are recorded. To be able to demonstrate the quantum nature of light, the angle of the second HWP is systematically adjusted at 5-degree intervals. The resulting counts registered by the detectors are documented as data files.

Upon completion of data collection, an in-depth analysis ensues, aiming to determine whether the observed light behavior aligns with quantum particle characteristics. This assessment is facilitated by evaluating the second-order correlation function $g^{(2)}(0)$. We have the following expression for $g^{(2)}(0)$

$$g^{(2)}(0) = \frac{P_{ABB'}(0)}{P_{AB}(0)P_{AB'}(0)} \tag{2.1}$$

The probabilities can be easily acquired using conditional probability to give the following

$$P_{AB}(0) = \frac{N_{AB}(0)}{N_A}$$

$$P_{AB'}(0) = \frac{N_{AB'}(0)}{N_A}$$

$$P_{ABB'}(0) = \frac{N_{ABB'}(0)}{N_A}$$

These can be plugged into (2.1) to give the final expression for the quantum coherence factor

$$g^{(2)}(0) = \frac{N_A N_{ABB'}}{N_{AB} N_{AB'}} \tag{2.2}$$

We must also consider the fact that there is a statistical error associated with having a finite time window, however small it may be. What is meant by this is that since we have a detection time window of 10 ns, if 2 photons have a time difference of detection

that is less than 10 ns, the processor will count them as being coincident, even if they are not. They are statistically determined and the corresponding coherence factor due to accidental counts is also retrieved.

- Probability of accidental coincidence:

$$P'_{ABB'} = P_{AB}N_{B'}\Delta t + P_{AB'}N_B\Delta t$$

- $g^{(2)}(0)$ due to accidental counts:

$$g'^{(2)}(0) = N_A\Delta t(\frac{N_{B'}}{N_{AB'}} + \frac{N_B}{N_{AB}})$$

The $g^{(2)}(0)$ must come out to be around 0 to prove that we have observed the 'grainy-ness' of the light beam. Upon calculation, we can confirm that it does, as shown in figure 2.

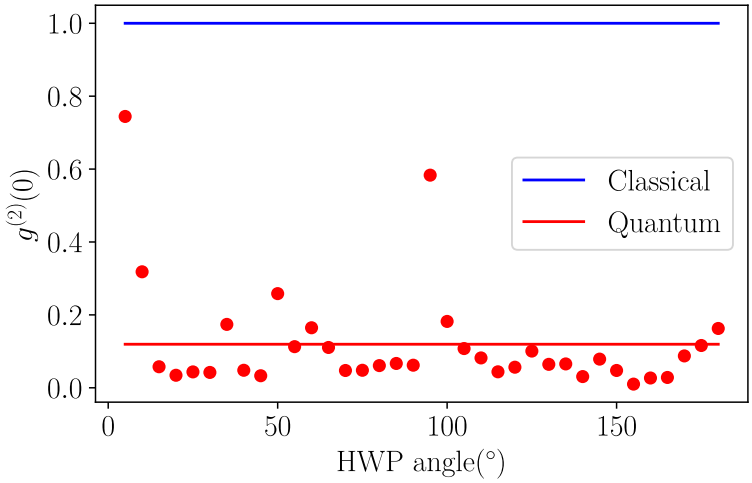

Figure 2: Experimentally found quantum $g^{(2)}(0)$ and the ideal case of classical $g^{(2)}(0)$.

With that confirmed we must then move on to prove that the states of the photons outgoing from the BBO are entangled. For this, we conduct the CHSH test of local realism.

2.1.1 CHSH test

The next key experiment is used to confirm entanglement and is the CHSH test, aiming to scrutinize the adherence or violation of local realism. The testing parameter under consideration was the quantity denoted as S, as defined in equation 2.3:

$$S = E(a,b) - E(a,b') + E(a',b) + E(a',b'), \tag{2.3}$$

where $E(x,y)$ represents the expected outcome of a local realistic measurement for the analysis angle of x in channel A (signal) and y in channel B (idler), as specified in equation 2.4:

$$E(x,y) = \cos(2(x-y)). \tag{2.4}$$

The CHSH inequality is then expressed as $|S| \leq 2$ under the assumptions of locality, reality, and hidden variable arguments.

Violation of this inequality, with $|S| > 2$, contradicts the predictions of local realism and implies non-local behavior. For an entangled state, such as Φ^+, the theoretical value of S is $S_{\text{th}} = 2\sqrt{2}$. This theoretical value establishes the upper limit of the CHSH inequality under the assumption of non-locality.

Given experimental constraints, precisely generating the maximally entangled state Φ^+ can be challenging. Therefore, the experimental determination of S is expected to lie within the range defined by the following equation:

$$2 < S_{\text{exp}} < 2\sqrt{2}. \tag{2.5}$$

This range encapsulates the conditions for a successful violation of the CHSH inequality, providing evidence of non-locality in accordance with quantum mechanics. The analysis involves calculating the theoretical value of S for the specified analysis angles ($a = -45°$, $a' = 0°$, $b = 22.5°$, $b' = -22.5°$) and comparing it with the experimentally determined value, emphasizing the importance of achieving results beyond the classical bounds imposed by local realism.

The setup for the experiment is shown in figure 3. We must now achieve maximal violation of CHSH identity. To establish the Bell state, it is imperative to balance the counts for AB and A'B' while minimizing A'B and AB' counts in both the $\{|H, V\rangle$, $|V, H\rangle\}$ and $\{|D, A\rangle$, $|A, D\rangle\}$ bases. Minimizing A'B and AB' counts in both bases implies setting ϕ to zero.

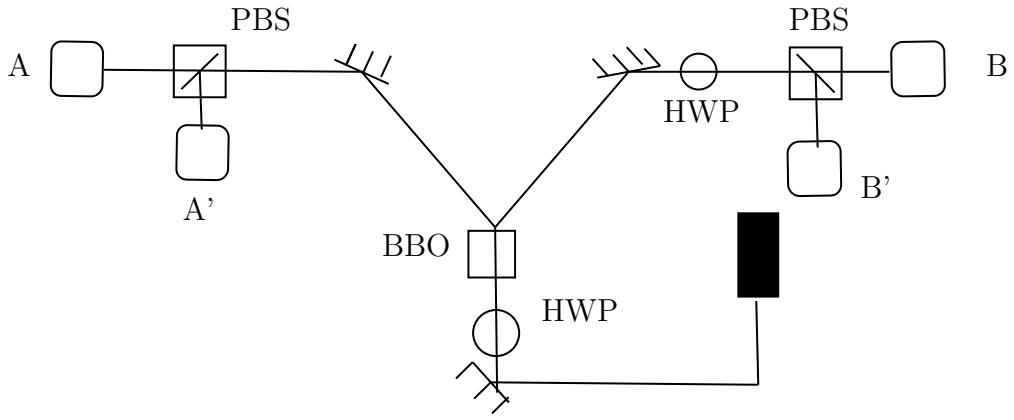

Figure 3: Four detector setup for the CHSH test.

Firstly, we construct the $\{|HV\rangle$, $|VH\rangle\}$ measurement basis. The HWP angles for A and B are set to 0°. In this configuration, the A and B detectors record horizontally polarized photons emitted by the source, and the A' and B' detectors register vertically polarized photons. The pump beam HWP is adjusted until the AB and A'B' coincidences are maximized, maintaining a ratio close to 1:1, while ensuring that A'B and AB' coincidences are minimized.

Subsequently, the measurement basis is switched to $\{|DA\rangle$, $|AD\rangle\}$ by setting the HWP angles for A and B to 22.5°, and the tilt of the quartz plate is adjusted to minimize the A'B and AB' coincidences. The AB and A'B' coincidences should remain

maximized and approximately equal in number.

To refine the state further, a few iterations of the aforementioned steps are performed. Ultimately, when the AB and A'B' coincidences are approximately in a 1:1 ratio, and A'B and AB' coincidences are minimized in both measurement bases, the down-converted photons are generated in the desired Bell state.

After data has been collected, it is utilized to ascertain the probabilities referenced in equation 2.4. These probabilities, in turn, facilitate the determination of $E(a, b)$, $E(a, b')$, $E(a', b)$, and $E(a', b')$. The values for each of these expectation values comes out to be:

$$E(a, b) = 0.554 \pm 0.001$$

$$E(a, b') = -0.577 \pm 0.001$$

$$E(a', b) = 0.607 \pm 0.001$$

$$E(a', b') = 0.678 \pm 0.001$$

Once $E(x, y)$ had been established for each set of analysis angle pairs, equation 2.3 enables the calculation of the experimental value of S, denoted as S_{exp}. Our value of S_{exp} comes out to be:

$$S_{exp} = 2.514 \pm 0.002$$

which agrees well with what we had expected. This confirmation attests that the photon pairs in question were entangled and demonstrated a violation of local realism. This is evident as the CHSH inequality 2.5 has been breached by our observed value of S_{exp}.

2.2 Experimental Setup to Reconstruct a Ghost Image

There are some necessary arrangements to be made to be able to achieve a fully reconstructed ghost image. A photon source, in our case a laser beam being sent through a BBO crystal, is used to generate entangled photon pairs through a process called spontaneous parametric down-conversion (SPDC). An 405 nm wavelength photon is split into two lower-energy (810 nm) entangled photons. In SPDC, a single photon is incident on the non-linear crystal, and it can split into two entangled photons. The tensor product is a mathematical operation used to combine two quantum states to describe a composite system. These two photons are created in such a way that their properties are correlated, and they share quantum entanglement. If we denote the state of the first photon as $|\psi_1\rangle = V$ and the state of the second photon as $|\psi_2\rangle = V$, then the joint or composite state of the two photons is given by the tensor product of $|\psi_1\rangle$ and $|\psi_2\rangle$:

$$|\Psi\rangle = |\psi_1\rangle \otimes |\psi_2\rangle = V \otimes V.$$

After the entangled photons are produced, they are sent in different directions. One photon (called the signal photon) is sent to the object or scene being imaged, for which we use a spatial light modulator (SLM) to add amplitude change to the photon beam as a representation of the object. The other photon (called the idler photon) is directed towards an SLM that adds a series of random masks to the idler photon and then sends this 'masked' photon to the detector. The signal photon interacts with

the object, and its properties are changed based on this interaction.

Our system for spatially resolving detection is implemented through the utilization of a spatial light modulator (SLM), where a sequence of random binary patterns, known as masks, is displayed. Subsequently, the projection formed by these masks is captured by a bucket detector. The measured correlations offer insights into the similarity or overlap between the object and each applied mask. The process involves scanning through a series of these masks, and the duration of this scanning operation scales with the necessary resolution for the imaging task at hand. The spatial light modulator plays a crucial role in dynamically adapting the patterns, contributing to the versatility of the system in capturing detailed spatial information. This methodology provides a mechanism for extracting meaningful data about the object. The idler photon, which does not interact with the object, serves as a reference. The idler and signal photon beams are detected by a bucket detector. The correlation between the detected idler photons and the signal photons that interacted with the object is then analyzed. This correlation is a crucial quantum feature and is typically established through a coincidence measurement.

Despite the fact that the idler photons alone do not carry detailed spatial information, the correlations between the signal and idler photons can be used to reconstruct an image of the object. This is achieved through computational algorithms that exploit the quantum correlations to extract the spatial information. The resolution of the reconstructed image is determined by the number of pixels on the SLM as well as the number of masks used [6]. However, one limitation is the inefficient imaging speed, as the number of measurements needed for reconstruction scales quadratically with the required resolution (i.e. we are putting more masks in front of the beam to extract more information and therefore have a higher number of computations performed). An visual of the planned setup is shown in figure 4.

2.2.1 Masks

Let us now delve a little deeper into the use of masks within the aforementioned setup [6]. Consider the intensity of the output signal of the bucket detector to be B_r which is given by

$$B_r = \int \int I_r(x, y)T(x.y)\mathrm{d}x\mathrm{d}y, \tag{2.6}$$

where $I_r(x, y)$ is the r-th random pattern illuminated on an object and $T(x.y)$ is the transmittance of the object. Since we use a discrete number of masks to, we must also discretize the above equation. The intensity B_r detected through measurement of the (i, j)th mask is given by

$$B_r = \sum_{p=1}^{N} \sum_{q=1}^{N} I_{ijpq} T_{pq} \tag{2.7}$$

where $n = N^2$ is the total number of illuminations and NxN is the resolution of our mask. The higher we want the resolution to be, the greater our n will become, thus increasing the number of masks we must apply. This must be carefully considered considering the computation time will increase with the number of masks.

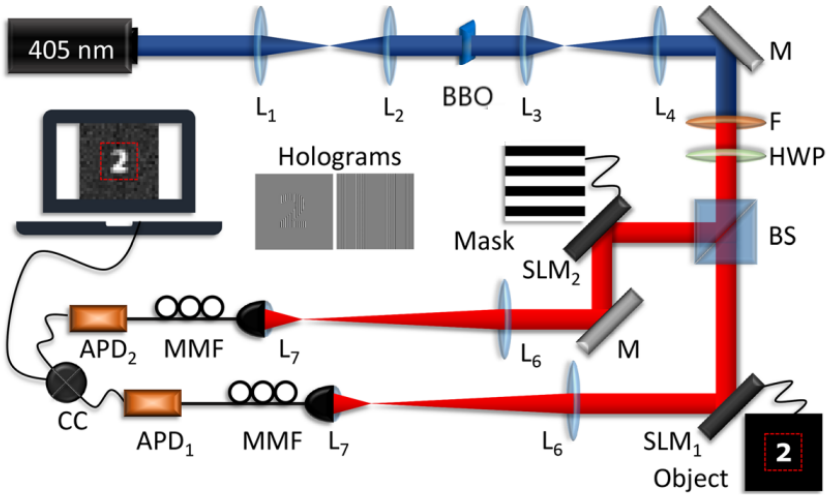

Figure 4: Setup to create a ghost image [1]. The elements labeled L_1 to L_7 are lenses used to focus the respective photon beams. The element labeled M is a mirror and HWP is a half-wave plate. The beam splitter (labelled BS) is used to split the idler beam and signal beam. After the respective beams pass through the object and mask SLMs, they are detected by the bucket detectors. Through these, coincidences are recorded and processed and we thus have a final reconstruction of the object as a ghost image.

2.2.2 A Brief Mathematical Formulation

Let us now draw out this process step-by-step for a 2×2 system with ideal conditions (no noise or attenuation). We first have the composite state $V_I \otimes V_S$ (I represents idler beam and S represents signal beam) which looks like this in vector form:

$$V = \begin{bmatrix} 0 \\ 0 \\ 0 \\ 1 \end{bmatrix} \tag{2.8}$$

We then add the object to the idler beam and the masks to the signal beam. Since we are in the composite Hilbert space, these operations will take the following shape:

$$\hat{O}' = \hat{O}_I \otimes \hat{I}_S \tag{2.9}$$

$$\hat{M'}_{i,j} = \hat{I}_I \otimes \hat{M}_{S_{i,j}} \tag{2.10}$$

since we are applying the object (represented by operator $\hat{O}'$) to the idler beam and the mask (represented by operator $\hat{M}$) to the signal beam. The indices (i, j) on the mask operator represent the pixel that it is being applied to. For each mask we will generate a random matrix of binary values. For example:

$$\mathbf{M} = \begin{bmatrix} 0 & 0 & 1 & 0 \\ 1 & 1 & 0 & 0 \\ 0 & 0 & 0 & 1 \\ 0 & 1 & 0 & 1 \end{bmatrix} \tag{2.11}$$

A series of masks like this will be applied to the signal beam according to the required resolution. The application of the masks can be visualized as in figure 5.

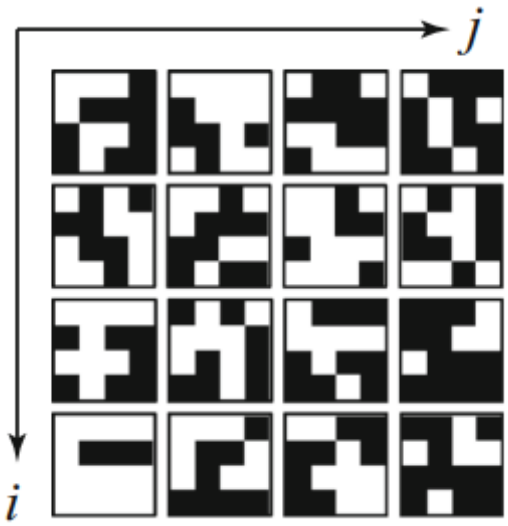

Figure 5: Binary illumination masks used for ghost imaging [6].

The object can also be represented as a 4×4 matrix of arbitrary amplitudes.

$$\mathbf{O} = \begin{bmatrix} a & 0 & 0 & 0 \\ 0 & b & 0 & 0 \\ 0 & 0 & c & 0 \\ 0 & 0 & 0 & d \end{bmatrix} \tag{2.12}$$

These operators will be applied on the V composite photon state. After the operators have been applied, we will take measurement and get probability amplitudes. The probability values will give us information about the object.

3 Next Course of Action

What is left to discuss now is the next step within this endeavor. We try to give a debriefing here of what the plan to move forward is. A paramount focus during this stage is to ensure that the observed results align with our anticipated outcomes. Rigorous confirmation and validation processes will have be employed to ascertain the reliability and accuracy of the obtained data. Additionally, measures will be taken to address any unforeseen variables or deviations, thereby enhancing the robustness of the experimental framework.

3.1 Building the framework

The crucial next step is to gather all the materials required for the experimental set so that we may perform the experiment and see if the results match our predictions. If they do not, any necessary changes would then be provided and implemented.

3.2 Data Processing

While processing the data for analysis, the number of masks to implement would have to be decided. This will depend on the SLM as well as the resolution of the image we wish to construct. The SNR ratio will also be evaluated for our obtained results.

3.3 Refining results

After the previous steps have been established, we can implement an AI-based model to further enhance our image without adding any noise. Resizing an image to a higher resolution is inherently lossy, resulting in the loss of fine details. Similarly, when experimentally reconstructing a higher resolution image in a ghost imaging experiment, the process leads to exponentially long image reconstruction times. To address these challenges in a two-fold manner, neural networks are employed. This involves initially reconstructing the image at a low resolution, followed by denoising and super-resolving to achieve a high resolution. This approach not only ensures efficient measurement times but also enhances the output to up to four times the measured resolution [1].

4 Conclusion

In this document, we have discussed the basics behind ghost imaging as well as some of the preliminary quantum mechanics needed to be able to have a deeper understanding of what we are trying to achieve. An overview of the setup and processing methods has been given for how we will reconstruct the ghost image. The next step is to put the blueprint in action and determine if our results match the predictions.

References

[1] C. Moodley and A. Forbes, "Super-resolved quantum ghost imaging," *Scientific Reports*, vol. 12, no. 1, p. 10346, 2022. [Online]. Available: https://doi.org/10.1038/s41598-022-14648-2

[2] M. D'Angelo and Y. H. Shih, "Quantum imaging," *Laser Physics Letters*, vol. 2, no. 12, p. 567, sep 2005. [Online]. Available: https://dx.doi.org/10.1002/lapl.200510054

[3] H. Defienne, B. Ndagano, A. Lyons, and D. Faccio, "Polarization entanglement-enabled quantum holography," *Nature Physics*, vol. 17, no. 5, pp. 591–597, 2021. [Online]. Available: https://doi.org/10.1038/s41567-020-01156-1

[4] Y. Shih, "Quantum imaging," *IEEE Journal of Selected Topics in Quantum Electronics*, vol. 13, no. 4, pp. 1016–1030, 2007.

[5] S. Anwar, *Quantum Mechanics in the Single Photon Laboratory*. IOP Publishing, 2020, pp. 4–1–5–26.

[6] K. Shibuya, K. Nakae, Y. Mizutani, and T. Iwata, "Comparison of reconstructed images between ghost imaging and hadamard transform imaging," *Optical Review*, vol. 22, no. 6, pp. 897–902, 12 2015. [Online]. Available: https://doi.org/10.1007/s10043-015-0138-x